ACS APPLIED MATERIALS & INTERFACES

Research Article

www.acsami.org

Ultrathin TiO_2 Layer Coated-CdS Spheres Core–Shell Nanocomposite with Enhanced Visible-Light Photoactivity

Zhang Chen and Yi-Jun Xu*

State Key Laboratory Breeding Base of Photocatalysis, College of Chemistry and Chemical Engineering, Fuzhou University, Fuzhou, Fujian 350002, P.R. China

College of Chemistry and Chemical Engineering, New Campus, Fuzhou University, Fuzhou, Fujian 350108, P.R. China

Supporting Information

ABSTRACT: Development of various strategies for controllable fabrication of core–shell nanocomposites (CSNs) with highly active photocatalytic performance has been attracting ever-increasing research attention. In particular, control of the ultrathin layer TiO_2 shell in constructing CSNs in an aqueous phase is a significant but technologically challenging issue. Here, this paper demonstrates the interface assembly synthesis of CdS nanospheres@TiO_2 core–shell photocatalyst via the electrostatic interaction of negatively charged water-stable titania precursor with positively charged CdS nanospheres (CdS NSPs), followed by the formation of the ultrathin-layer TiO_2 shell through a facile refluxing process in aqueous phase. The as-formed CdS NSPs@TiO_2 core–shell nanohybrid exhibits a high visible-light-driven photoactivity for selective transformation and reduction of heavy metal ions. The ultrathin TiO_2 layer coated on CdS NSPs results in excellent light transmission property, enhanced adsorption capacity, and improved transfer of charge carriers and lifespan of photoinduced electron–hole pairs, which would prominently contribute to the significant photoactivity enhancement. It is anticipated that this facile aqueous-phase synthesis strategy could be extended to design a variety of more efficient CSN photocatalysts with controllable morphology toward target applications in diverse photoredox processes.

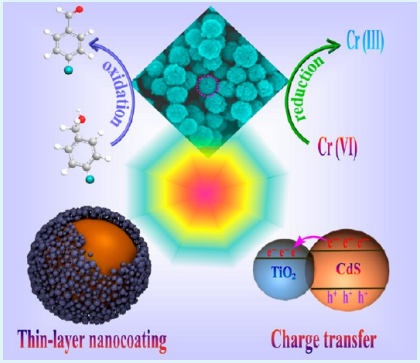

KEYWORDS: *core–shell nanocomposites, ultrathin layer coating, interface assembly, electrostatic interaction, selective photoredox*

INTRODUCTION

The eternal pursuit for sustainable energy and a pollutant-free environment keeps moving. In this context, photocatalysis is a promising and significant process for energy storage and conversion to chemical energy.[1] It is of great interest and importance to efficiently design and exploit photocatalysts that can operate well under solar light for practical application in environmental and clean energy areas.[2−9] Recently, core–shell nanocomposite (CSN) photocatalysts have drawn great interest due to their unique properties and promising potential for energy conversion.[10] Roughly speaking, there are five kinds of CSNs that have been prepared so far, i.e., semiconductor@semiconductor, metal@semiconductor, metal@metal, CNT@semiconductor, and metal or semiconductor core@inactive shell (C, SiO_2, polyaniline).[10−13] Hitherto, CSN photocatalysts are primarily utilized for "nonselective" degradation of dyes and volatile toxic pollutants, overall photolysis of water, and independent hydrogen evolution.[12−24] Although some pioneering research works about selective photocatalytic aerobic oxidation of alcohols by TiO_2 photocatalysts have been reported by Palmisano's group[25,26] and Zhao's group,[27,28] research works on utilizing CSN photocatalysts for "selective" redox reactions are relatively scarce.[10] In recent years, synthesis of the noble metal@semiconductor CSNs (e.g., Pt@CeO_2, Pd@CeO_2, Pd@CdS, Pd@hollow CeO_2) as visible-light photocatalysts for selective reduction of aromatic nitro compounds and selective oxidation of a series of alcohols has been reported by our group.[29−32] In addition, Tsai et al.[33] have reported the use of core–shell Ni@NiO/$InTaO_4$–N nanohybrid for photocatalytic reduction of carbon dioxide. As faithfully testified by these research works, CSN photocatalysts have immense potential for heterogeneous photocatalytic selective redox processes. However, it should be noted that the application of semiconductor core@semiconductor shell composites in photocatalytic selective redox reactions has still been relatively scarce. In view of the fact that core–shell architectures could offer a great opportunity for tuning the interaction among the different components in ways that might improve catalytic activity or structural stability,[34] it is reasonable to believe that coating semiconductor substrate with other semiconductor particles to form semiconductor core@semiconductor shell CSNs with controllable structural morphology might provide greater versatility in performing selective photoredox processes.

However, rational selection of semiconductor precursors in fabricating ultrathin semiconductor shell to form CSNs with uniform morphology always represents a technologically challenging issue. This is particularly prominent for the case

Received: October 1, 2013
Accepted: November 18, 2013
Published: November 18, 2013

of controllable shell coating of semiconductor TiO_2 for the fabrication of semiconductor@TiO_2 CSNs in an aqueous phase. The reason is that the precursors of TiO_2 shell are often titanium alkoxides or titanium chloride with a very rapid hydrolysis rate and even hydrolyze instantly when exposed to moisture, often leading to uncontrollable precipitation of TiO_2 in aqueous solution and aggregation of the coated TiO_2 particles.[35−40] The drawback of these titania precursors provides a challenge for achieving the ultrathin TiO_2 shell coating in the synthesis of semiconductor core@TiO_2 shell nanocomposites in an aqueous phase. To address this problem, the previous attention has been paid to slowing down the hydrolyzation speed of these titania precursors via the addition of assistant reagents (e.g., the surfactant, polymer, or polyelectrolyte) or controlling the dropping rate of water in the synthetic process.[16,35−38] However, these synthetic routes, which often demand relatively complex experimental procedures, are performed in organic or mixed phase and are difficult to scale up for practical applications. Furthermore, as compared to preparation in organic or mixed phase, controllable synthesis of nanomaterials in aqueous phase is provided with many advantages, e.g., environmental friendliness, biocompatibility, water solubility, and low cost.[41] Thereby, it is highly urgent to exploit a new and simple strategy for fabricating TiO_2-based CSNs in an aqueous phase.

As a significant member of semiconductor@semiconductor CSNs, the CdS@TiO_2 CSN photocatalysts with a controllable, ultrathin layer thickness of TiO_2 shell and high photoactivity for selective redox reactions have been seldom reported. With regard to the case of CdS@TiO_2 CSNs, the presence of ultrathin TiO_2 shell can improve the light transmission capacity and less reflectance of visible light would be realized. However, how to obtain the ultrathin-layer TiO_2 shell of TiO_2-based CSNs is often technologically difficult in an aqueous phase. Recently, Lou and his co-workers have reported that the thin carbon coating on CdS could improve visible-light photoactivity toward degradation of dyes.[42] It is therefore of interest to develop suitable surface engineering methods to design efficient core−shell photocatalysts. In this regard, coating CdS with an ultrathin layer of TiO_2 shell may be an effective method to improve both the light transmission capacity and photocatalytic performance. Importantly, in view of the matchable energy band position between TiO_2 and CdS, the shell of TiO_2 nanoparticles coated onto the CdS core matrix might result in efficient photoinduced charge carriers transfer, which is distinctly different from the carbon coating onto CdS.[42]

Toward this end, we herein demonstrate a new, simple, and viable strategy for fabrication of semiconductor CdS nanospheres@semiconductor TiO_2 core−shell nanocomposite (CSN) via an interface self-assembly process and its utilization as a highly efficient visible-light photocatalyst for selective organic transformations and environmental remediation. The use of titanium(IV) bis(ammonium lactato)dihydroxide (TALH), a water-stable titania precursor, can realize an easy control of ultrathin layer coating of TiO_2 shell onto the CdS core. Dressing the CdS core with such an ultrathin TiO_2 layer can efficiently improve the lifespan and transfer of photoinduced electrons from CdS core to the surface of TiO_2 shell, thereby leading to the high photocatalytic efficiency for photoredox reactions over CdS nanospheres@TiO_2 CSNs. Thus, this work not only shows a simple ultrathin layer coating strategy for controllable aqueous phase synthesis of highly efficient CdS NSPs@TiO_2 CSN with improved photoactivity but also highlights the prospective scope to develop the potential applications of CSNs in photocatalytic selective transformation for fine chemicals synthesis and reduction of heavy metal ions for environmental remediation.

EXPERIMENTAL SECTION

Materials. Thiourea (NH_2CSNH_2), cadmium acetate dihydrate ($Cd(CH_3COO)_2{\cdot}2H_2O$), ethanol ($C_2H_6O$), (3-aminopropyl) triethoxysilane ($C_9H_{23}NO_3Si$, APTES), ammonium oxalate, $AgNO_3$, benzoquinone, and *tert*-butyl alcohol were purchased from Sinopharm Chemical Reagent Co., Ltd. Additionally, titanium(IV) bis(ammonium lactato)dihydroxide was obtained from Alfa Aesar. Deionized water was from local sources. All reagents were analytical grade and used without further purification.

Synthesis. The CdS NSPs@TiO_2 CSN photocatalyst has been prepared by a simple yet efficient interface self-assembly method, followed by the formation of TiO_2 shell through a facile refluxing process.

(I) Synthesis of CdS Nanospheres (CdS NSPs). Uniform CdS NSPs were fabricated via a simple hydrothermal method,[43,44] as illustrated in Scheme S1 (Supporting Information). The details for preparing CdS NSPs are presented in the Supporting Information.

(II) Fabrication of CdS NSPs@TiO_2 CSN by the Interface Assembly of TiO_2 Nanoparticles on the Surface of CdS NSPs. Amine-functionalized CdS NSPs were prepared via a facile refluxing method[44] and presented for the following reaction. Negatively charged titanium(IV) bis(ammonium lactato)dihydroxide (TALH) 50% w/w aqueous solution (0.4 g) was added into positively charged CdS NSP (0.15 g) dispersion. After being vigorously stirred at pH = 6 for 30 min, the mixed suspension was refluxed at 100 °C for 24 h, which allowed the formation of TiO_2 shell. The solution was then cooled to room temperature. Finally, the yellow precipitate was centrifuged and washed with distilled water and then dried in an oven at 60 °C.

Characterization. The Fourier transformed infrared spectroscopy (FTIR) was carried out on a Nicolet Nexus 670 FTIR spectrophotometer at a resolution of 4 cm^{-1}. Zeta potential (ξ) measurements of the samples were performed by dynamic light scattering analysis (Zeta sizer 3000HSA) at room temperature (ca. 25 °C) according to the previous works.[44,45] The crystal phase properties of the samples were analyzed with a Bruker D8 Advance X-ray diffractometer (XRD) using Ni-filtered Cu Kα radiation at 40 kV and 40 mA in the 2θ, ranging from 5° to 80° with a scan rate of 0.02° per second. Field-emission scanning electron microscopy (FESEM) was used to determine the morphology of the samples on a FEI Nova NANOSEM 230 spectrophotometer. Transmission electron microscopy (TEM), high-resolution transmission electron microscopy (HRTEM) images, and energy-dispersive X-ray spectroscopy (EDX) were obtained using a JEOL model JEM 2010 EX instrument at an accelerating voltage of 200 kV. X-ray photoelectron spectroscopy (XPS) measurements were carried out on a Thermo Scientific ESCA Lab250 spectrometer which consists of a monochromatic Al Kα as the X-ray source, a hemispherical analyzer, and sample stage with multiaxial adjustability to obtain the surface composition of the sample. The optical properties of the samples were analyzed by UV−vis diffuse reflectance spectroscopy (DRS) using a UV−vis spectrophotometer (Cary 500, Varian Co.). Raman spectroscopic measurements were performed on a Renishaw inVia Raman System 1000 with a 532 nm Nd:YAG excitation source at room temperature. The Brunauer−Emmett−Teller (BET) specific surface area (S_{BET}) of the samples was analyzed by nitrogen adsorption in a Micromeritics ASAP 2020 apparatus. The electrochemical impedance spectroscopy (EIS) experiments were conducted on a Precision PARC workstation. The photoluminescence (PL) spectra for solid samples were measured on an Edinburgh FL/FS900 spectrophotometer under an excitation wavelength at 468 nm. Electron spin resonance (ESR) spectra were investigated using a Bruker A300 EPR electron paramagnetic resonance spectrometer, and the irradiation wavelength was >420 nm, the same light source as that for the photocatalytic redox reactions.

Scheme 1. Scheme Illustrating Interface Assembly Synthesis of CdS Nanospheres@TiO_2 CSN

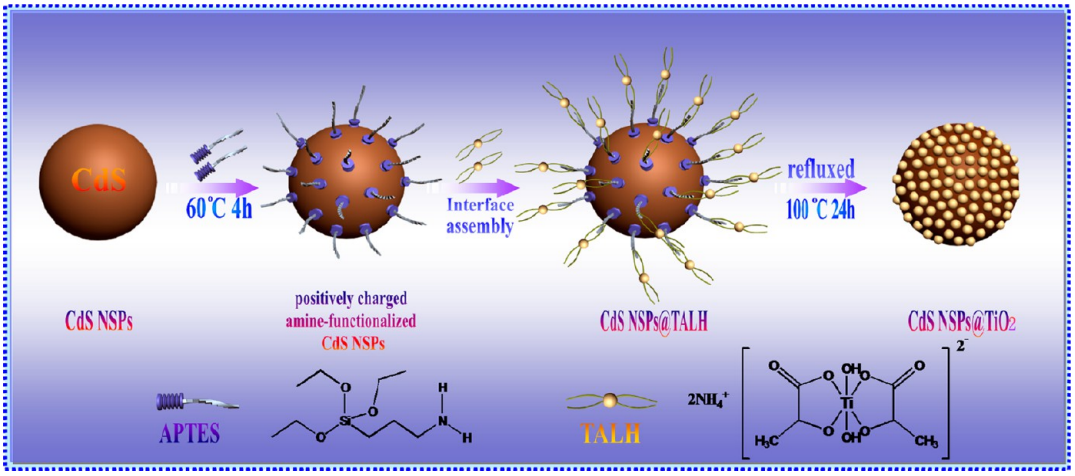

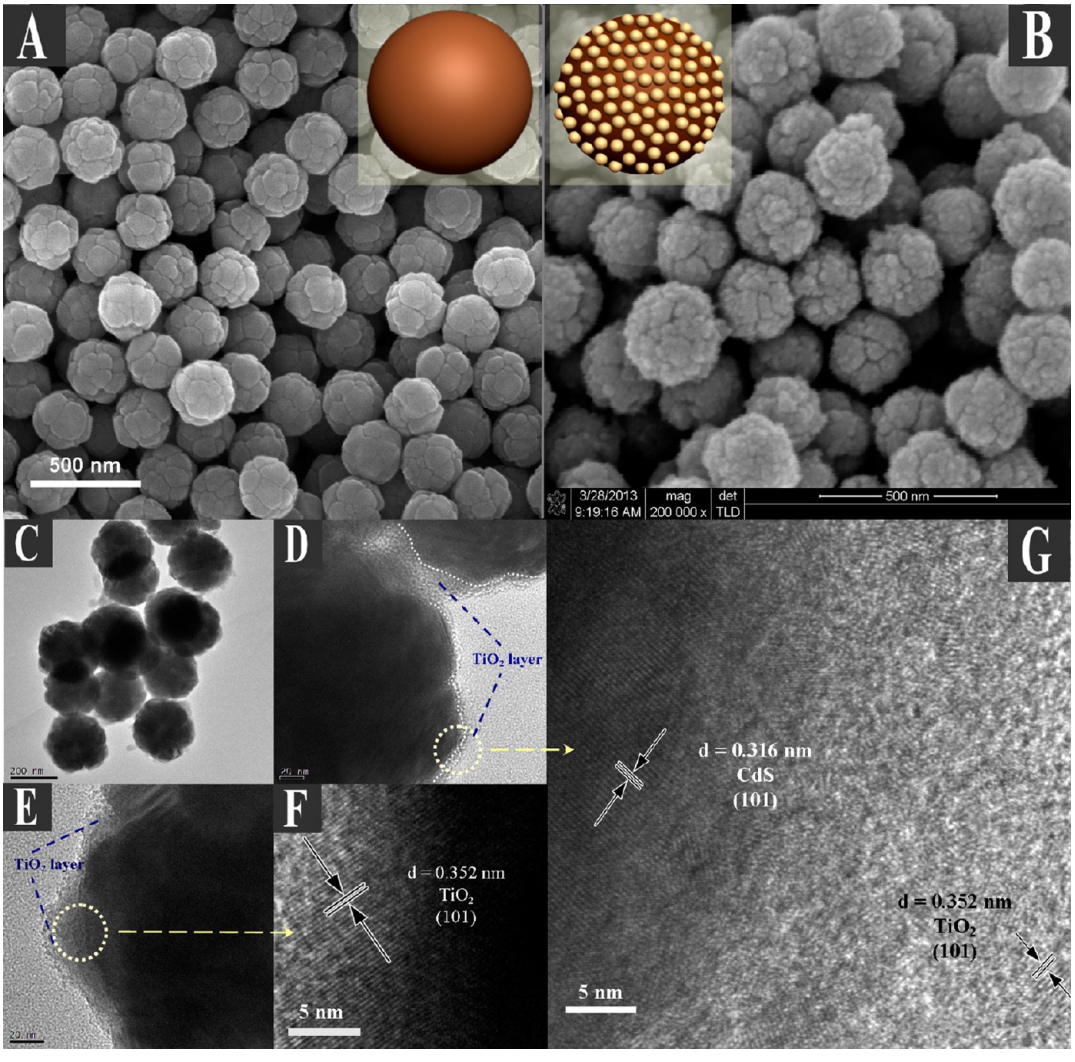

Figure 1. SEM images of (A) bare CdS NSPs and (B) CdS NSPs@TiO_2 CSN (the insets of A and B are the corresponding model illustrations). (C–E) TEM images and (F,G) HRTEM images of CdS NSPs@TiO_2 CSN.

Catalyst Performance. Photocatalytic selective oxidation of alcohols to corresponding aldehydes was carried out as in previous research works.[27−31,46−49] The tests of photocatalytic performance for selective oxidation of alcohols are presented in the Appendix of the Supporting Information. Controlled photoactivity experiments using different radical scavengers (ammonium oxalate as photogenerated holes scavenger,[46,47,50] $AgNO_3$ as electrons scavenger,[46,47,51] benzoquinone as superoxide radical species scavenger,[52,53] and *tert*-butyl alcohol as hydroxyl radical species scavenger[46,47]) were performed according to the previous research works.[46,47] Conversion of alcohol,

yield of aldehyde, and selectivity for aldehyde were calculated as the follows:

$$\text{conversion } (\%) = [(C_0 - C_{\text{alcohol}})/C_0] \times 100$$

$$\text{yield } (\%) = C_{\text{aldehyde}}/C_0 \times 100$$

$$\text{selectivity } (\%) = [C_{\text{aldehyde}}/(C_0 - C_{\text{alcohol}})] \times 100$$

where C_{alcohol} and C_{aldehyde} are, respectively, the concentration of the substrate alcohol and the corresponding aldehyde at a certain time after the photocatalytic reaction, and C_0 is the initial concentration of alcohol.

As to photocatalytic reduction of Cr(VI) to Cr(III), the photoactivity was performed in light of previous research works.[54] The tests of photocatalytic performance for reduction of Cr(VI) are also presented in the Appendix of the Supporting Information.

RESULTS AND DISCUSSION

A schematic diagram of the interface self-assembly formation of CdS NSPs@TiO_2 CSN is illustrated in Scheme 1. In the first stage, the CdS NSPs prepared by a facile hydrothermal method[43,44] are refluxed in ethanol with the addition of (3-aminopropyl)triethoxysilane (APTES). The positively charged CdS NSPs are obtained by the modification of APTES, endowing the surface of CdS full of amine functional groups. This is precisely corroborated by the FTIR spectra (Figure S1, Supporting Information) and Zeta potential analysis (Figure S2A, Supporting Information). Following removal of the excess APTES after centrifugation and ethanol washing of the particles, the amine-functionalized CdS NSPs are exposed to an aqueous solution to get homogeneous suspension by ultrasonication. Then, TALH, a chelating compound provided with the carboxyl groups,[39,55−58] is added to the suspension. The adsorption of negative charged TALH (Figure S2B, Supporting Information) on the surface of amine-functionalized CdS NSPs would occur, which could establish a solid and valid basis for such an interface self-assembly strategy. Subsequently, refluxing of the TALH-coated CdS NSPs particles results in the formation of three-dimensional (3D) CdS NSPs@TiO_2 CSN. The success of this method for forming the CdS NSPs@TiO_2 core−shell hybrid relies on the utilization of water-stable TALH that can be assembled with APTES. While titanium alkoxides or titanium chloride hydrolyze rapidly in the existence of water, TALH is stable at ambient temperature in neutral solution.[39,55,58] Significant hydrolysis and condensation reactions could be effectively suppressed via using TALH as titania precursor, which can further prevent precipitation of TiO_2 in aqueous solution and possible aggregation of the coated TiO_2 particles. Therefore, TALH is an ideal candidate for use in controllable interface engineering as it can be deposited and hydrolyzed in a uniform way. Furthermore, as compared to preparation using titanium alkoxides in organic or mixed phase, controllable synthesis of TiO_2-based CSNs via using TALH in aqueous phase possesses several merits, e.g., environmental friendliness, biocompatibility, water solubility, and low cost.[41] More importantly, it is conceivable that such an interface assembly method by using TALH holds significant potential to construct TiO_2-based core−shell photocatalysts in aqueous phase for photocatalytic target reactions.

The field-emission scanning electron microscopy has been utilized to directly analyze the morphology of the CdS NSP@TiO_2 CSN. From the comparison of Figure 1A,B, we could clearly observe that nanosized TiO_2 particles are uniformly decorated on the CdS NSPs substrate, suggesting that the core−shell structure with close interfacial contact between two components is constructed. The morphology and structure of these particles are further elucidated by transmission electron microscopy (TEM), as shown in Figure 1C−E. An ultrathin TiO_2 layer enwrapped in the CdS NSPs strongly confirms the formation of core−shell architecture, which is well consistent with the SEM results. Figure 1F,G displays the high-resolution TEM (HRTEM) images of CdS NSPs@TiO_2 CSN. The identified lattice spacings of 0.352 and 0.316 nm in HRTEM images correspond to the (101) facet of TiO_2 and (101) facet of CdS, respectively. Moreover, the energy-dispersive X-ray analysis (Figure 2A,B) on the selected interfacial area between

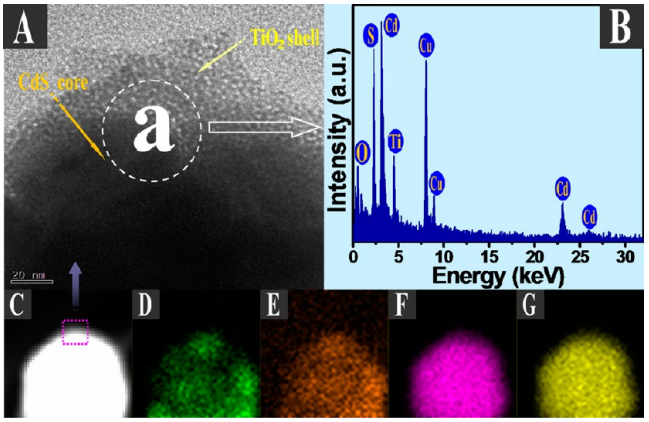

Figure 2. (A) Typical TEM image, (B) the EDX spectrum for selected interfacial area between the ultrathin TiO_2 shell and CdS core in CdS NSPs@TiO_2 CSN, (C) the high angle annular dark field-scanning transmission electron microscopy image and mapping results of the elements (D) Ti, (E) O, (F) Cd, and (G) S.

the TiO_2 shell and CdS core demonstrates clearly that the CdS NSPs@TiO_2 CSN composites contain Ti, O, Cd, and S elements. To further corroborate the formation of CdS NSPs@TiO_2 core−shell structure, the elemental mapping has also been carried out to disclose the element distribution in the CdS NSPs@TiO_2 spheres, as shown in Figure 2C−G. The results elucidate that the Ti, O, Cd, and S elements exist in the composite and the distribution range of TiO_2 is slightly larger than that of CdS located in the inner center of the spheres, which confirms the ultrathin-layer TiO_2 nanocoating onto the CdS core for the CdS NSPs core@TiO_2 shell structure nanocomposites and is well consistent with the TEM and HRTEM analysis in Figure 1.

As confirmed by the above SEM, TEM, and elemental mapping results, interfacial engineering of CdS NSPs@TiO_2 CSN can be achieved by such a simple assembly approach, which offers a doable way for coating semiconductor nanoparticles with a thin-layer TiO_2 shell. To further demonstrate the superiority and efficiency of this facile strategy, a set of comparative experiments has been performed using CdS NSPs without any pretreatment of amine-functionalized CdS NSPs, as depicted in Figure 3. In Route (I), the amine-functionalized CdS NSPs can be readily assembled with TALH; then after refluxing, the core−shell architecture with uniform TiO_2 shell coating is obtained. Nevertheless, the CdS NSPs in Route (II) go through no pretreatment and fail to interact well with TALH, thus resulting in few scattered TiO_2 nanoparticles decorated with CdS NSPs after refluxing. Thus, it is clear that our current, rational interface self-assembly strategy has a

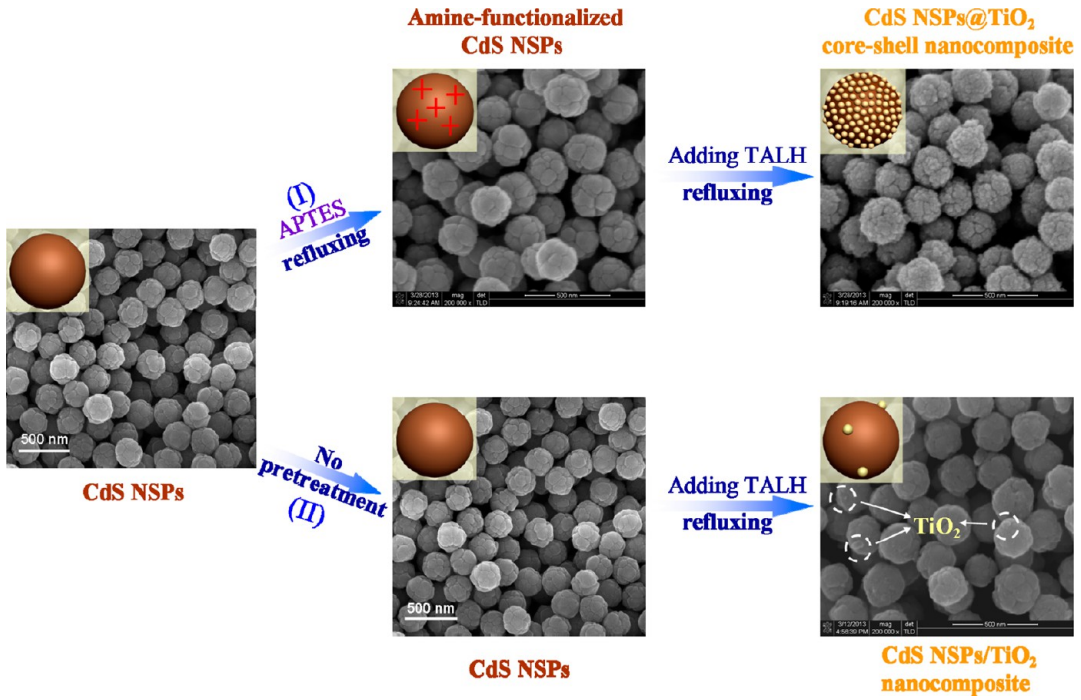

Figure 3. Synthetic flowchart for (I) interface assembly synthesis of CdS NSPs@TiO_2 core−shell nanohybrid and (II) direct synthesis of CdS NSPs−TiO_2 nanocomposite without pretreatment of CdS NSPs by APTES.

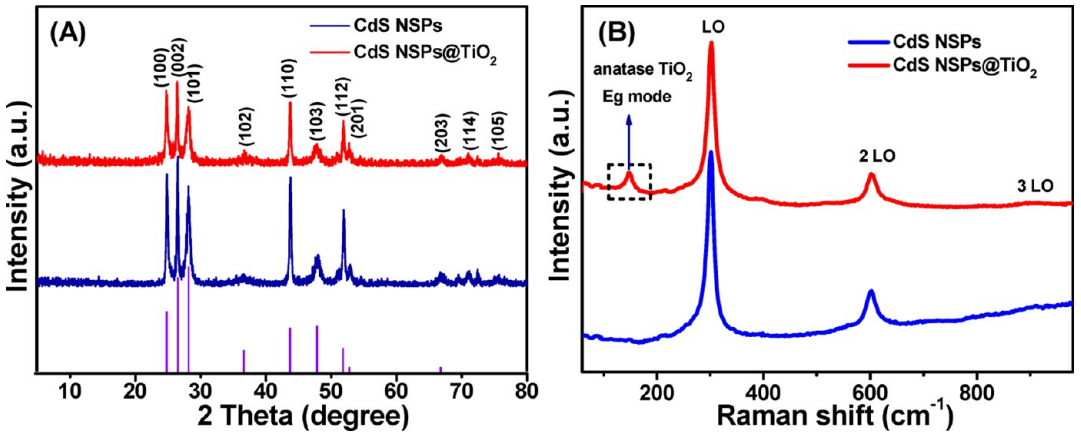

Figure 4. (A) XRD patterns and (B) Raman spectra (532 nm laser excitation wavelength) at room temperature of bare CdS NSPs and CdS NSPs@ TiO_2 CSN.

prominent advantage in a controllable manner, thereby leading to the formation of TiO_2-based CSNs with a uniform morphology and thin layer shell coating.

The XRD diffraction peaks (Figure 4A) of the CdS NSPs and CdS NSPs@TiO_2 CSN are all in accordance with a hexagonal CdS phase (JCPDS #41-1049). The characteristic diffraction peaks for TiO_2 could not be seen from the pattern due to its relatively low diffraction intensity. Besides, the (100) peak of hexagonal CdS might also overlap with the primary characteristic peak of TiO_2 at approximately 25.4°. Nevertheless, the presence of TiO_2 can be verified by the Raman analysis. As depicted in Figure 4B, the characteristic Raman mode of the TiO_2 nanoparticles coated on CdS NSPs can be readily identified as compared to the pure CdS NSPs. The results demonstrate that the formation of an anatase TiO_2 is evident from the low frequency anatase Eg mode (ca. 146 cm^{-1}) with low intensity,[59] manifesting that the TiO_2 with poor crystallization can be achieved through refluxing treatment at 100 °C. In addition, the resonantly excited longitudinal optical (LO) phonon of CdS NSPs locates at ca. 300 cm^{-1}, and resonant excitations located at 604 and ca. 900 cm^{-1} correspond to the first (2 LO) and second (3 LO) overtones of the CdS NSPs, respectively.[60,61]

Further evidence for ultrathin TiO_2 layer coated-CdS NSPs could come from the XPS analysis. Obvious photoelectron peaks of Ti, O, Cd, and S elements are observed in the XPS survey spectra (Figure S3, Supporting Information) for the surface of CdS NSPs@TiO_2 CSN. It can be observed from Figure 5A that two typical peaks of Ti 2p located at approximately 459.2 and 464.8 eV correspond to the Ti $2p_{3/2}$ and Ti $2p_{1/2}$ binding energies,[62−64] respectively. The O 1s peak in Figure 5B could be further divided into two different peaks with binding energy at ca. 530.7 and 532.2 eV, which could be ascribed to the Ti−O in TiO_2 and hydroxyl groups,

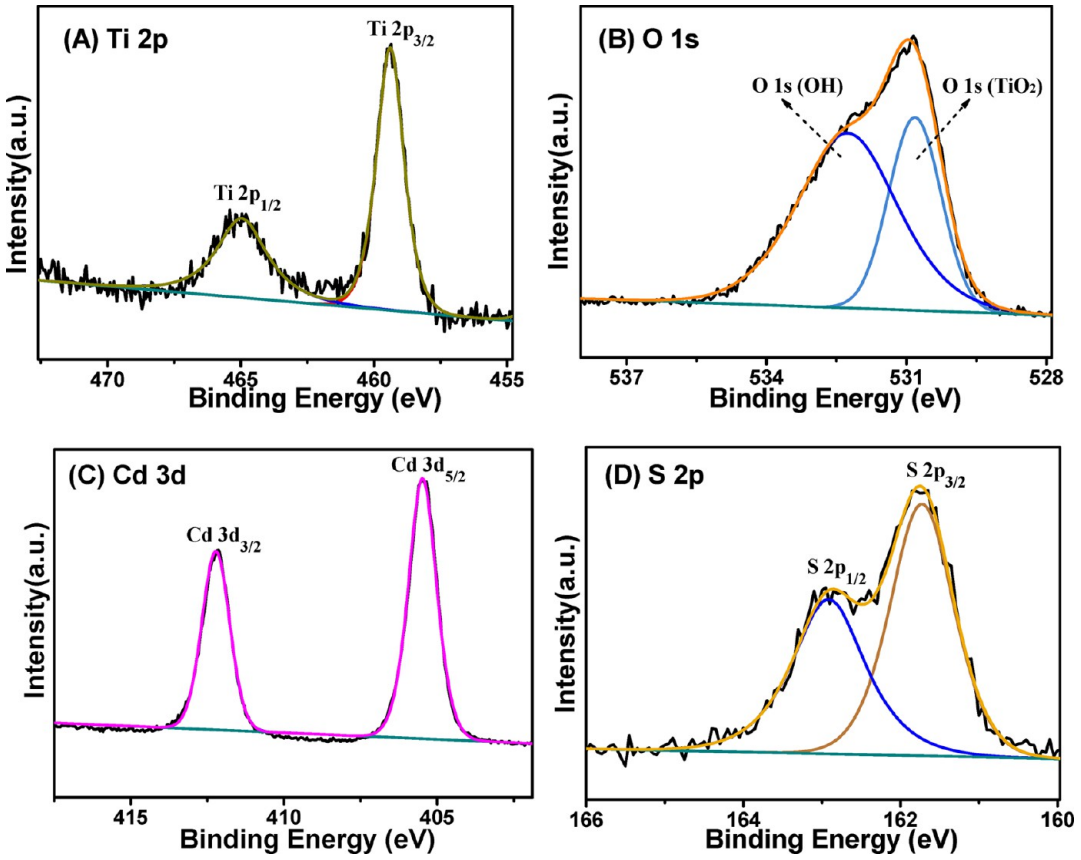

Figure 5. XPS analysis of the as-obtained CdS NSPs@TiO_2 CSN: the peak deconvolution for (A) Ti 2p, (B) O 1s, (C) Cd 3d, and (D) S 2p.

respectively.[63,64] The spectra of Cd 3d in Figure 5C show two different peaks Cd $3d_{5/2}$ and Cd $3d_{3/2}$ with binding energies 405.5 and 412.2 eV, respectively.[62] The S 2p spectrum in Figure 5D includes two individual peaks S $2p_{3/2}$ and S $2p_{1/2}$ with respective binding energies 161.6 and 162.8 eV, indicating that the valence state of element S is −2.[31,65] As known to all, the elements for core in the CSNs can not generally be analyzed by the XPS surface analysis (its detection depth is usually <10 nm) unless the thickness of shell is thin enough. Herein, the Cd and S elements of CdS core can be observed by XPS, which is clearly due to the ultrathin TiO_2 shell nanocoating in good accordance with the TEM results.

For investigating the optical properties of the photocatalysts, a comparison of the UV−vis diffuse reflectance spectra over CdS NSPs and CdS NSPs@TiO_2 CSN is depicted in Figure 6. An enhanced absorbance in the ultraviolet region can be observed after incorporation of CdS NSPs with TiO_2, thus allowing more efficient utilization of the solar energy for trigging chemical redox reactions. This is understandable because TiO_2 by itself has strong UV light absorption. It could be deduced from the joint SEM and TEM analysis that most of the visible light could transmit through the ultrathin TiO_2 shell, thus leading to no evident decrease in the absorption capacity of visible light over CdS NSPs@TiO_2 CSN despite TiO_2 having no visible-light absorption. In addition, slight variation in the band gap is observed from the inset of Figure 6. More specifically, the band gap over CdS NSPs@TiO_2 CSN is approximately 2.29 eV, which is narrowed slightly in comparison with that of pure CdS nanospheres at 2.31 eV. The results indicate that both CdS nanopheres and CdS nanospheres@TiO_2 CSN can be photoinduced under the

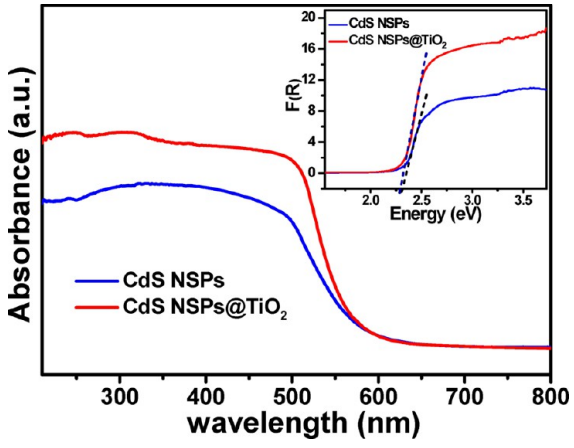

Figure 6. UV−vis diffuse reflectance spectra of the as prepared CdS NSPs and CdS NSPs@TiO_2 CSN (the inset is the plot of transformed Kubelka−Munk function vs the energy of light).

illumination of visible light, by which photocatalytic redox reactions can be driven.

The photocatalytic performance of CdS NSPs and CdS NSP@TiO_2 CSN toward selective redox reactions, i.e., photocatalytic oxidation of alcohols and reduction of Cr(VI), has been investigated under visible-light illumination. It can be observed obviously, from Figures 7 and 8 and Table S1 (Supporting Information), that CdS NSPs@TiO_2 CSN demonstrates significantly improved photocatalytic performance in comparison with blank CdS NSPs for selective redox reactions. Therefore, we can draw the conclusion that coating CdS NSPs with an ultrathin TiO_2 layer could lead to the

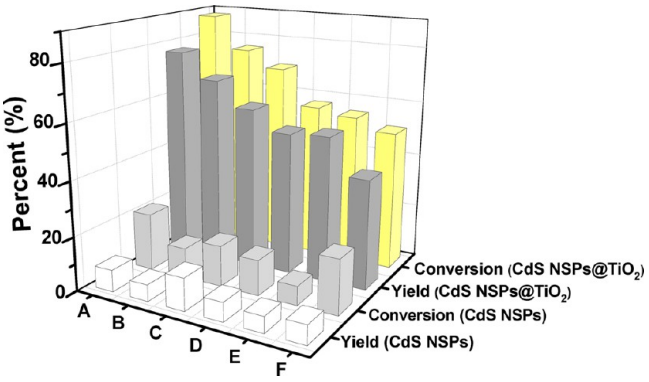

Figure 7. Photocatalytic selective oxidation of alcohols to corresponding aldehydes over the CdS NSPs and CdS NSPs@TiO_2 CSN photocatalysts under visible-light irradiation (λ > 420 nm) for 2h under ambient conditions: (A) *p*-chloro benzyl alcohol, (B) *p*-methyl benzyl alcohol, (C) *p*-methoxyl benzyl alcohol, (D) *p*-fluoro benzyl alcohol, (E) benzyl alcohol, and (F) 3-methyl-2-buten-1-ol.

obvious photoactivity enhancement toward selective redox reactions. The results indicate that the effective interfacial hybridization between CdS NSPs and TiO_2 contributes to the remarkably enhanced photoactivity, thus making CdS NSPs@TiO_2 CSN be an efficient photocatalyst for selective redox reactions.

The aim of investigating the reasons for obvious photoactivity enhancement toward selective redox reactions over the photocatalysts, the surface area measurement, photoluminescence (PL) spectra, and electrochemical impedance spectra (EIS) has been performed. The Brunauer–Emmett–Teller (BET) surface areas and porous structures over CdS NSPs@TiO_2 CSN and pure CdS NSPs have been investigated using nitrogen adsorption–desorption experiments (Table S2, Supporting Information). The results indicate that ultrathin TiO_2 nanocoating onto CdS NSPs results in a larger surface area than that of bare CdS NSPs. The photoactivity enhancement of photocatalysts is often related to a larger specific surface area, which could provide more surface active sites, resulting in enhanced adsorptivity for reactants and improved transfer of charge carriers.[66,67] Therefore, coating TiO_2 on the matrix of CdS NSPs might play an important role in improving the photoactivity. In addition, the difference in the adsorptivity toward reactants can be confirmed by the adsorption experiments for benzyl alcohol and Cr(VI). It can be concluded from Figure 9 that the existence of TiO_2 nanocoating could enhance the adsorptivity toward reactants, which might contribute to the actions of selective redox processes.

It is well established that CdS and TiO_2 are provided with matchable energy band position, together with intimate interfacial contact confirmed by our TEM results, which is able to result in the efficient charge carriers transfer. This reference is verified by the PL spectra and electrochemical impedance spectra. It can be evidently observed from Figure S4 (Supporting Information) that the obviously lower emission intensity over CdS NSP@TiO_2 than pure CdS NSPs represents an effective interfacial charge-transfer process, which could be primarily ascribed to the efficient transfer of electrons from the conduction band (CB) of CdS NSPs to the CB of TiO_2. Moreover, it can be obviously seen from Nyquist impedance plots (Figure S5, Supporting Information) that the CdS NSP@TiO_2 CSN shows depressed semicircles at high frequencies as compared to blank CdS nanospheres, suggesting that the charge-transfer resistance decreases.[68,69] Therefore, a consensus is reached that the integration of CdS NSPs with TiO_2 could improve the transfer of charge carriers, thereby efficiently hampering the recombination of electron–hole pairs.

A sequence of controlled experiments using different radical scavengers has been carried out in order to deeply understand the role of photogenerated radical species in the photocatalytic oxidation of alcohols over the photocatalysts. The results of adding different radical scavengers over CdS NSPs and CdS NSPs@TiO_2 reaction systems under the illumination of visible light are shown in Figure 11. When the radical scavengers, ammonium oxalate (AO) for holes,[46,47,50] $AgNO_3$ for electrons[46,47,51] and benzoquinone (BQ) for superoxide radicals ($O_2^{\bullet-}$)[52,53] are added into the two reaction systems, the conversion of benzyl alcohol and the yield of benzaldehyde remarkably decrease, manifesting that the selective oxidation of benzyl alcohol is mainly related to photoinduced holes, electrons (the activation of molecular oxygen to form active oxygen species, e.g., $O_2^{\bullet-}$), and $O_2^{\bullet-}$. In particular, the presence of $O_2^{\bullet-}$ has been confirmed by the electron spin resonance (ESR) spectra. As shown in Figure 10, six characteristic peaks of the DMPO-$O_2^{\bullet-}$ adducts are both observed on CdS NSPs@TiO_2 CSN and CdS NSPs suspensions in the BTF solution under visible-light irradiation. In contrast, no obvious signals

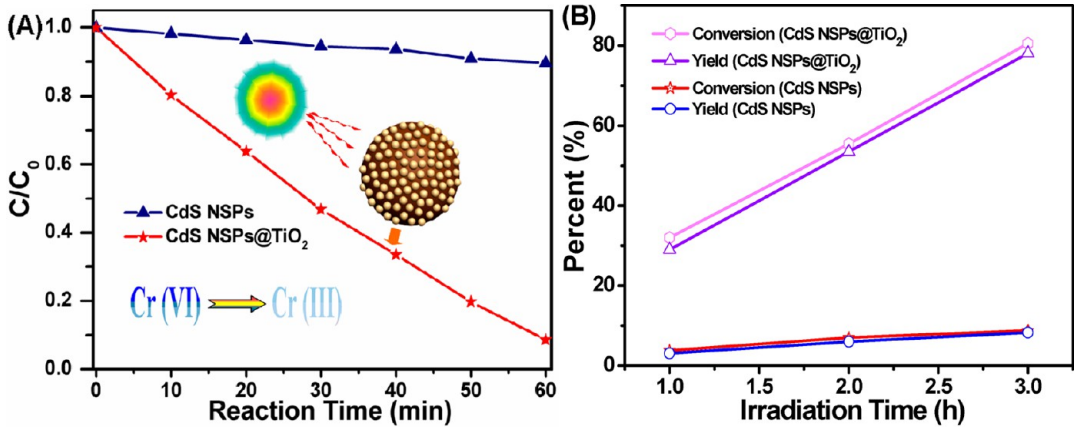

Figure 8. (A) Photocatalytic reduction of Cr(VI) and (B) results of time-online profiles of photocatalytic selective oxidation of benzyl alcohol over pure CdS NSPs and CdS NSPs@TiO_2 CSN under the visible-light illumination (λ > 420 nm).

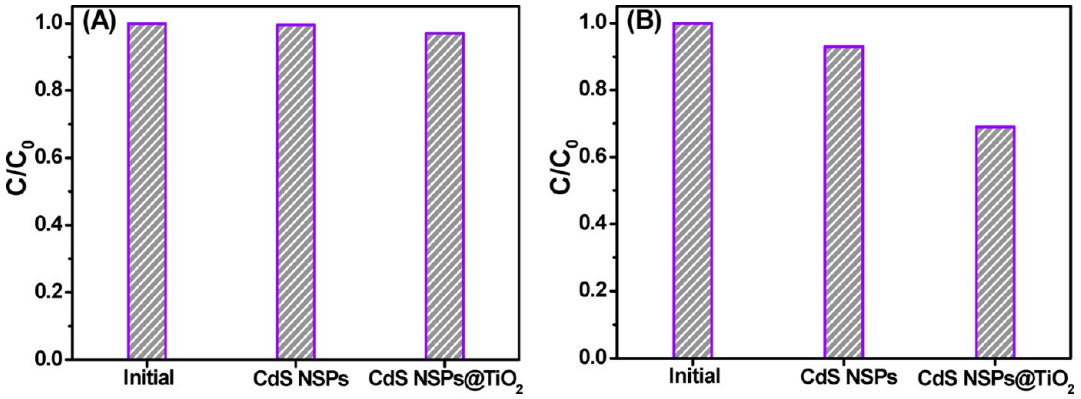

Figure 9. Column plots showing the remaining (A) benzyl alcohol and (B) Cr(VI) in solution after being kept in the dark for 2 h until adsorption equilibrium of the reactants solution over pure CdS nanospheres and CdS nanospheres@TiO_2 CSN.

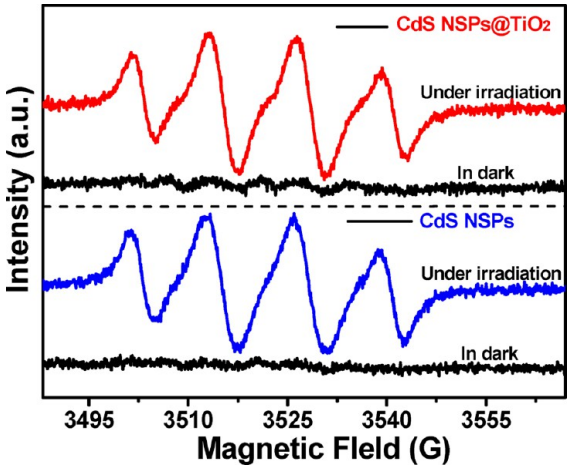

Figure 10. ESR spectra of radical adducts trapped by DMPO (DMPO-$O_2^{\bullet-}$) over CdS NSPs@TiO_2 CSN and CdS NSPs suspensions with or without the illumination of visible light.

are detected in the dark. The results elucidate that $O_2^{\bullet-}$ is generated in the reaction systems over CdS NSPs@TiO_2 CSN and CdS NSPs under visible-light illumination. During the oxidation reaction, it is worth noting that the photogenerated holes in the CdS NSPs@TiO_2 system can also contribute to selective oxidation of benzyl alcohol, which can be due to the ultrathin TiO_2 shell enhancing the adsorption for alcohols and not suppressing the contact of the alcohols with the holes from CdS core, thus making the holes take part in oxidation of alcohols. Moreover, the photocatalytic conversion and yield over CdS NSPs@TiO_2 CSN are almost unaffected by the addition of *tert*-butyl alcohol (TBA) as scavenger for hydroxyl radical species,[46,47] which is similar to the observation over blank CdS NSPs, as reflected in Figure 11. This is consistent with the inexistence of hydroxyl radicals in the BTF solvent reported by the previous works.[28,48,70]

Figure 13 illustrates a tentative reaction mechanism proposed according to the above results. Under the illumination of visible light, the electrons (e^-) are photoexcited from the valence band of CdS NSPs to its conduction band, thus forming the electron−hole pairs. Subsequently, the photogenerated electrons could transfer to the conduction band of TiO_2 due to their matchable energy band position and intimate interfacial contact, thus resulting in the improved fate of photogenerated electron−hole pairs. As illustrated in Figure 12, the efficient two-level charge transfer from CdS to TiO_2 is formed under the illumination of visible light for photocatalytic reactions. With regard to the oxidation reaction, the photogenerated electrons can be accepted by molecular oxygen in the reaction system to form activated oxygen, e.g., $O_2^{\bullet-}$. The as-formed activated oxygen can oxidize the alcohols adsorbed on the surface of 3D CdS NSPs@TiO_2 CSNs to generate the corresponding aldehydes. Furthermore, on account of the ultrathin TiO_2 shell, the alcohols can also come into contact with the holes from CdS NSPs and be directly oxidized, which has been verified by the controlled experiments. As to the reduction process, the photogenerated electron across the surface of

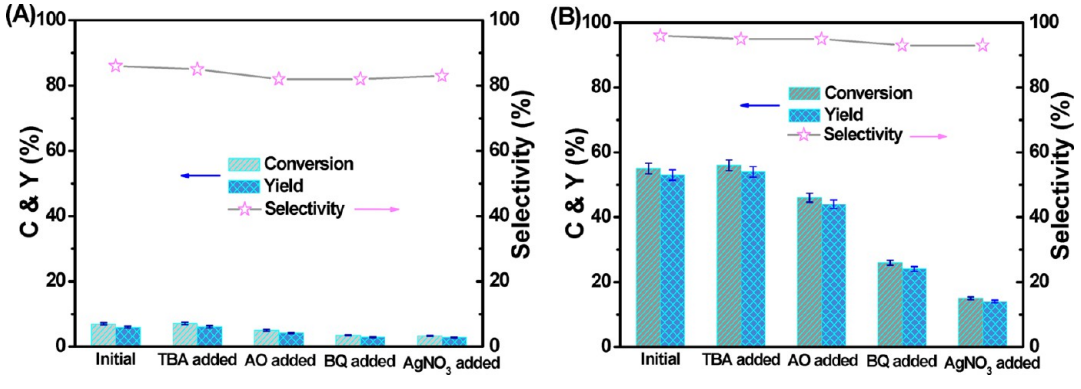

Figure 11. Controlled experiments using different radical scavengers for photocatalytic selective oxidation of benzyl alcohol over (A) CdS NSPs and (B) CdS NSPs@TiO_2 CSN under the illumination of visible light for 2 h.

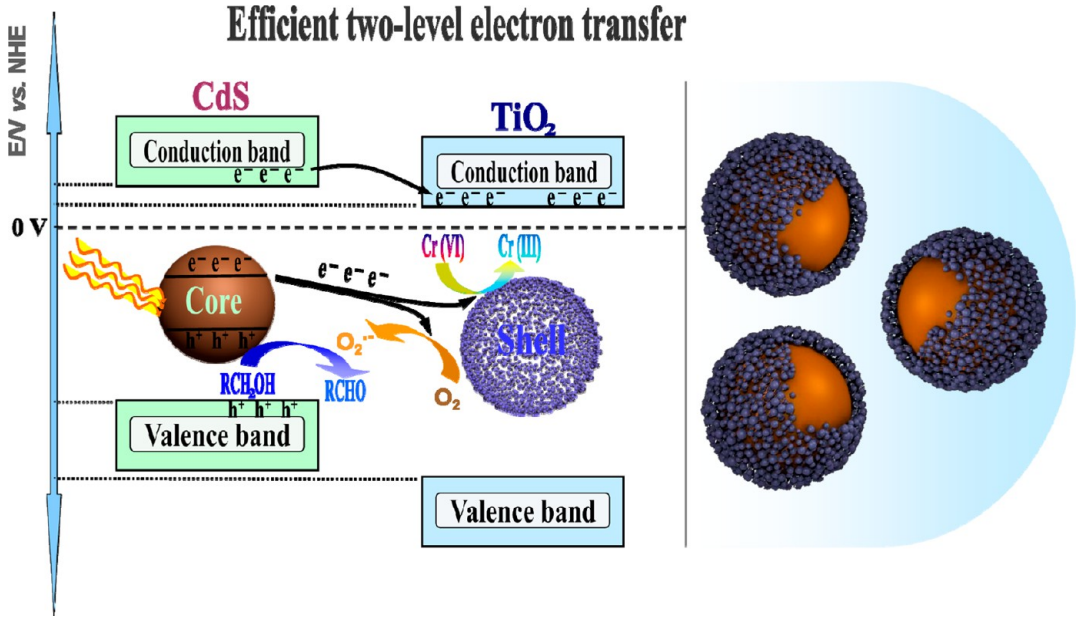

Figure 12. Scheme illustrating the transfer of charge carriers in CdS nanospheres@TiO_2 CSN under the visible-light illumination (λ > 420 nm).

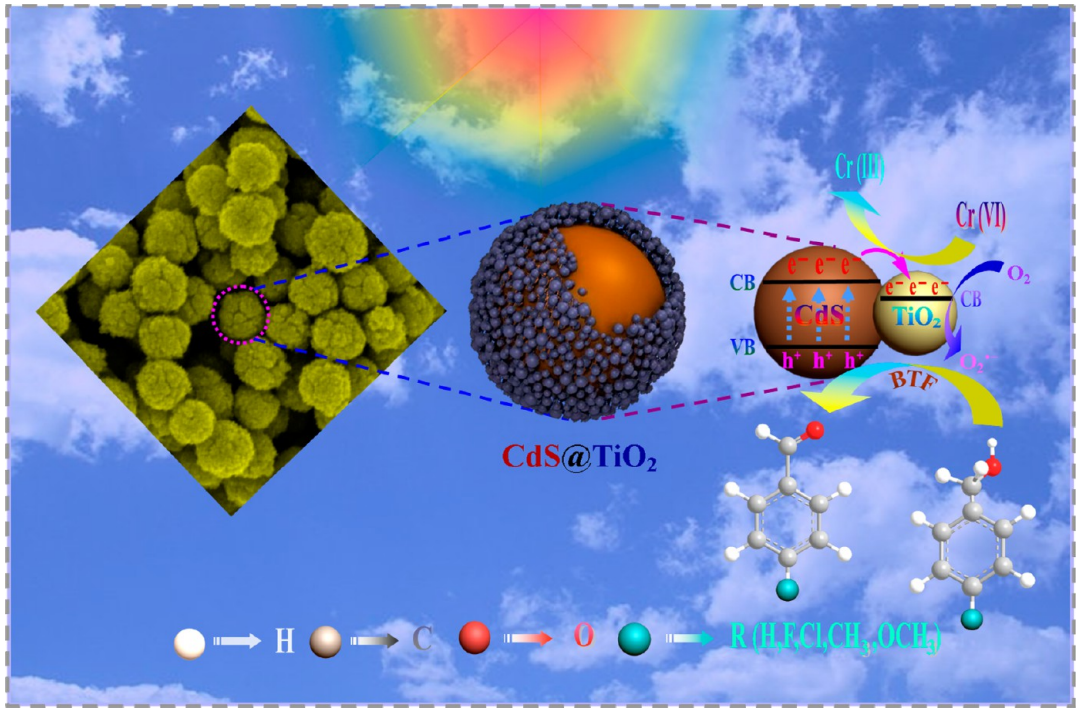

Figure 13. Scheme illustrating the proposed reaction mechanism for photocatalytic selective oxidation of a series of alcohols and reduction of Cr(VI) over the CdS nanospheres@TiO_2 CSN under the visible-light illumination.

photocatalysts could directly reduce the adsorbed Cr(VI) to Cr(III).

On the basis of the above discussions, it is necessary to make a scientific summary for the main effect of the thin TiO_2 layer coated on the CdS NSPs substrate in the CdS NSPs@TiO_2 CSN with remarkable photocatalytic performance enhancement. (I) The light transmission property of visible light can be optimized in the presence of the ultrathin TiO_2 layer nanocoating, by which more absorbance and less reflectance of visible light are achieved. (II) On account of the TiO_2 nanocoating, the resulted enhancement of surface area greatly enlarges the reaction space, thereby providing a sufficient opportunity of spatial contact between photocatalytic active species and reactants (alcohols and Cr(VI)). Moreover, the TiO_2 nanocoating onto CdS NSPs can also enhance the adsorption capacity of reactants. (III) The thin TiO_2 layer enwrapping CdS NSPs could efficiently accept the electrons to boost the separation of the photogenerated electron−hole pairs, thus effectively prolonging the fate of the charge carriers. To sum up, the above synthetic factors could give rise to the remarkably enhanced photoactivity of CdS nanospheres@TiO_2 CSN in comparison with pure CdS nanospheres.

dx.doi.org/10.1021/am4043068 | ACS Appl. Mater. Interfaces 2013, 5, 13353−13363

CONCLUSION

In summary, the rational engineering of CdS NSPs coated by the ultrathin TiO_2 layer with a core−shell structure has been realized via a facile interfacial self-assembly strategy, by which we for the first time use TALH to fabricate such a core−shell photocatalyst with a finely controllable uniform morphology and ultrathin-layer TiO_2 coating toward selective redox reactions. The TiO_2 nanocoating serves multiple functions, including tuning the light transmission capacity, enhancing adsorption capacity of reactants, and facilitating the separation of photogenerated charge carriers. As a result, the as-synthesized CdS NSPs@TiO_2 CSN, formed by the thin-layer TiO_2 nanoparticles encircling the CdS NSPs matrix, demonstrates excellent photocatalytic performance for selective redox reactions under visible-light irradiation. The simple design for encapsulating CdS NSPs core into the thin-layer TiO_2 shell could give rise to efficient two-level charge transfer and remarkable photoactivity enhancement during photocatalytic reactions. Hopefully, this work would inspire us to effectively utilize such a facile yet efficient interface assembly method to fabricate TiO_2-based CSNs by using TALH in aqueous phase and, more significantly, provide new advances into efficient design and utilization of CSNs as visible-light photocatalysts for a wide variety of selective transformations and environmental remediation.

ASSOCIATED CONTENT

Supporting Information

Schematic flowchart for hydrothermal preparation of CdS nanospheres, FTIR spectra of CdS nanospheres and amine-functionalized CdS nanospheres, zeta potentials analysis, XPS survey spectrum of the CdS nanospheres@TiO_2 CSN, details for selective oxidation of a series of alcohols to corresponding aldehydes under the visible-light illumination, BET surface area analysis, PL spectra of blank CdS nanospheres and CdS nanospheres@TiO_2 CSN under an excitation wavelength at 468 nm, EIS spectra of blank CdS NSPs and CdS NSPs@TiO_2 CSN under the visible-light illumination, and experimental details of photoactivity tests. This information is available free of charge via the Internet at http://pubs.acs.org.

AUTHOR INFORMATION

Corresponding Author

*Tel./Fax: +86 591 83779326. E-mail: yjxu@fzu.edu.cn.

Notes

The authors declare no competing financial interest.

ACKNOWLEDGMENTS

The support by National Natural Science Foundation of China (NSFC) (20903023, 21173045), the Award Program for Minjiang Scholar Professorship, the Natural Science Foundation (NSF) of Fujian Province for Distinguished Young Investigator Grant (2012J06003), Program for Changjiang Scholars and Innovative Research Team in Universities (PCSIRT0818), Program for Returned High-Level Overseas Chinese Scholars of Fujian province, and the Project Sponsored by the Scientific Research Foundation for the Returned Overseas Chinese Scholars, State Education Ministry, is gratefully acknowledged.

REFERENCES

(1) Fujishima, A.; Honda, K. *Nature* **1972**, *238*, 37−38.
(2) Chen, X.; Shen, S.; Guo, L.; Mao, S. S. *Chem. Rev.* **2010**, *110*, 6503−6570.
(3) Hoffmann, M. R.; Martin, S. T.; Choi, W.; Bahnemann, D. W. *Chem. Rev.* **1995**, *95*, 69−96.
(4) Linsebigler, A. L.; Lu, G.; Yates, J. T. *Chem. Rev.* **1995**, *95*, 735−758.
(5) Liu, G.; Niu, P.; Yin, L.; Cheng, H.-M. *J. Am. Chem. Soc.* **2012**, *134*, 9070−9073.
(6) Liu, G.; Wang, L.; Yang, H. G.; Cheng, H.-M.; Lu, G. Q. *J. Mater. Chem.* **2010**, *20*, 831−843.
(7) Maeda, K.; Teramura, K.; Lu, D.; Takata, T.; Saito, N.; Inoue, Y.; Domen, K. *Nature* **2006**, *440*, 295−295.
(8) Tada, H.; Kiyonaga, T.; Naya, S.-i. *Chem. Soc. Rev.* **2009**, *38*, 1849−1858.
(9) Zou, Z.; Ye, J.; Sayama, K.; Arakawa, H. *Nature* **2001**, *414*, 625−627.
(10) Zhang, N.; Liu, S.; Xu, Y.-J. *Nanoscale* **2012**, *4*, 2227−2238.
(11) Huang, X.; Li, Y.; Chen, Y.; Zhou, H.; Duan, X.; Huang, Y. *Angew. Chem., Int. Ed.* **2013**, *125*, 6179−6183.
(12) Lee, W. J.; Lee, J. M.; Kochuveedu, S. T.; Han, T. H.; Jeong, H. Y.; Park, M.; Yun, J. M.; Kwon, J.; No, K.; Kim, D. H.; Kim, S. O. *ACS Nano* **2011**, *6*, 935−943.
(13) Shanmugam, S.; Gabashvili, A.; Jacob, D. S.; Yu, J. C.; Gedanken, A. *Chem. Mater.* **2006**, *18*, 2275−2282.
(14) Ai, Z.; Zhang, L.; Lee, S.; Ho, W. *J. Phys. Chem. C* **2009**, *113*, 20896−20902.
(15) Awazu, K.; Fujimaki, M.; Rockstuhl, C.; Tominaga, J.; Murakami, H.; Ohki, Y.; Yoshida, N.; Watanabe, T. *J. Am. Chem. Soc.* **2008**, *130*, 1676−1680.
(16) Hirakawa, T.; Kamat, P. V. *J. Am. Chem. Soc.* **2005**, *127*, 3928−3934.
(17) Kuo, C.-H.; Yang, Y.-C.; Gwo, S.; Huang, M. H. *J. Am. Chem. Soc.* **2010**, *133*, 1052−1057.
(18) Lim, S. H.; Phonthammachai, N.; Pramana, S. S.; White, T. J. *Langmuir* **2008**, *24*, 6226−6231.
(19) Maeda, K.; Teramura, K.; Lu, D.; Saito, N.; Inoue, Y.; Domen, K. *Angew. Chem., Int. Ed.* **2006**, *118*, 7970−7973.
(20) Pan, C.; Xu, J.; Wang, Y.; Li, D.; Zhu, Y. *Adv. Funct. Mater.* **2012**, *22*, 1518−1524.
(21) Sakamoto, N.; Ohtsuka, H.; Ikeda, T.; Maeda, K.; Lu, D.; Kanehara, M.; Teramura, K.; Teranishi, T.; Domen, K. *Nanoscale* **2009**, *1*, 106−109.
(22) Wang, X.; Liu, G.; Lu, G. Q.; Cheng, H.-M. *Int. J. Hydrogen Energy* **2010**, *35*, 8199−8205.
(23) Yang, T.-T.; Chen, W.-T.; Hsu, Y.-J.; Wei, K.-H.; Lin, T.-Y.; Lin, T.-W. *J. Phys. Chem. C* **2010**, *114*, 11414−11420.
(24) Wang, S.; Wang, T.; Chen, W.; Hori, T. *Chem. Commun.* **2008**, *0*, 3756−3758.
(25) Yurdakal, S.; Palmisano, G.; Loddo, V.; Alagoz, O.; Augugliaro, V.; Palmisano, L. *Green Chem.* **2009**, *11*, 510−516.
(26) Yurdakal, S.; Palmisano, G.; Loddo, V.; Augugliaro, V.; Palmisano, L. *J. Am. Chem. Soc.* **2008**, *130*, 1568−1569.
(27) Zhang, M.; Chen, C.; Ma, W.; Zhao, J. *Angew. Chem., Int. Ed.* **2008**, *120*, 9876−9879.
(28) Zhang, M.; Wang, Q.; Chen, C.; Zang, L.; Ma, W.; Zhao, J. *Angew. Chem., Int. Ed.* **2009**, *48*, 6081−6084.
(29) Zhang, N.; Fu, X.; Xu, Y.-J. *J. Mater. Chem.* **2011**, *21*, 8152−8158.
(30) Zhang, N.; Liu, S.; Fu, X.; Xu, Y.-J. *J. Phys. Chem. C* **2011**, *115*, 22901−22909.
(31) Zhang, N.; Liu, S.; Fu, X.; Xu, Y.-J. *J. Mater. Chem.* **2012**, *22*, 5042−5052.
(32) Zhang, N.; Xu, Y.-J. *Chem. Mater.* **2013**, *25*, 1979−1988.
(33) Tsai, C.-W.; Chen, H. M.; Liu, R.-S.; Asakura, K.; Chan, T.-S. *J. Phys. Chem. C* **2011**, *115*, 10180−10186.
(34) Zhang, Q.; Lee, I.; Joo, J. B.; Zaera, F.; Yin, Y. *Acc. Chem. Res.* **2012**, *46*, 1816−1824.
(35) Liu, S.; Zhang, N.; Tang, Z.-R.; Xu, Y.-J. *ACS Appl. Mater. Interfaces* **2012**, *4*, 6378−6385.

(36) Chen, J. S.; Luan, D.; Li, C. M.; Boey, F. Y. C.; Qiao, S.; Lou, X. W. *Chem. Commun.* **2010**, *46*, 8252−8254.
(37) Joo, J. B.; Zhang, Q.; Dahl, M.; Lee, I.; Goebl, J.; Zaera, F.; Yin, Y. *Energy Environ. Sci.* **2012**, *5*, 6321−6327.
(38) Cheng, B.; Le, Y.; Yu, J. *J. Hazard. Mater.* **2010**, *177*, 971−977.
(39) Caruso, F.; Shi, X.; Caruso, R. A.; Susha, A. *Adv. Mater.* **2001**, *13*, 740−744.
(40) Xin, X.; Zhou, X.; Wu, J.; Yao, X.; Liu, Z. *ACS Nano* **2012**, *6*, 11035−11043.
(41) Gu, Z.; Zou, L.; Fang, Z.; Zhu, W.; Zhong, X. *Nanotechnology* **2008**, *19*, 135604.
(42) Hu, Y.; Gao, X.; Yu, L.; Wang, Y.; Ning, J.; Xu, S.; Lou, X. W. *Angew. Chem., Int. Ed.* **2013**, *125*, 5746−5749.
(43) Lin, G.; Zheng, J.; Xu, R. *J. Phys. Chem. C* **2008**, *112*, 7363−7370.
(44) Chen, Z.; Liu, S.; Yang, M.-Q.; Xu, Y.-J. *ACS Appl. Mater. Interfaces* **2013**, *5*, 4309−4319.
(45) Liu, S.; Chen, Z.; Zhang, N.; Tang, Z.-R.; Xu, Y.-J. *J. Phys. Chem. C* **2013**, *117*, 8251−8261.
(46) Zhang, N.; Zhang, Y.; Yang, M.-Q.; Tang, Z.-R.; Xu, Y.-J. *J. Catal.* **2013**, *299*, 210−221.
(47) Zhang, Y.; Zhang, N.; Tang, Z.-R.; Xu, Y.-J. *Chem. Sci.* **2012**, *3*, 2812−2822.
(48) Zhang, Y.; Tang, Z.-R.; Fu, X.; Xu, Y.-J. *ACS Nano* **2011**, *5*, 7426−7435.
(49) Tang, Z.-R.; Zhang, Y.; Xu, Y.-J. *ACS Appl. Mater. Interfaces* **2012**, *4*, 1512−1520.
(50) Carp, O.; Huisman, C. L.; Reller, A. *Prog. Solid State Chem.* **2004**, *32*, 33−177.
(51) Primo, A.; Marino, T.; Corma, A.; Molinari, R.; García, H. *J. Am. Chem. Soc.* **2011**, *133*, 6930−6933.
(52) Raja, P.; Bozzi, A.; Mansilla, H.; Kiwi, J. *J. Photochem. Photobiol., A* **2005**, *169*, 271−278.
(53) Stylidi, M.; Kondarides, D. I.; Verykios, X. E. *Appl. Catal., B* **2004**, *47*, 189−201.
(54) Zhang, N.; Yang, M.-Q.; Tang, Z.-R.; Xu, Y.-J. *J. Catal.* **2013**, *303*, 60−69.
(55) Baskaran, S.; Song, L.; Liu, J.; Chen, Y. L.; Graff, G. L. *J. Am. Ceram. Soc.* **1998**, *81*, 401−408.
(56) Guo, Y. G.; Hu, J. S.; Liang, H. P.; Wan, L. J.; Bai, C. L. *Adv. Funct. Mater.* **2005**, *15*, 196−202.
(57) Kimberly, N.; Yulin, D. *Nanotechnology* **2006**, *17*, 3219.
(58) Mockel, H.; Giersig, M.; Willig, F. *J. Mater. Chem.* **1999**, *9*, 3051−3056.
(59) Balaji, S.; Djaoued, Y.; Robichaud, J. *J. Raman Spectrosc.* **2006**, *37*, 1416−1422.
(60) Kontos, A.; Likodimos, V.; Vassalou, E.; Kapogianni, I.; Raptis, Y.; Raptis, C.; Falaras, P. *Nanoscale Res. Lett.* **2011**, *6*, 1−6.
(61) Sahoo, S.; Arora, A. K. *J. Phys. Chem. B* **2010**, *114*, 4199−4203.
(62) Wu, L.; Yu, J. C.; Fu, X. *J. Mol. Catal. A: Chem.* **2006**, *244*, 25−32.
(63) Yu, J. C.; Yu, J.; Tang, H. Y.; Zhang, L. *J. Mater. Chem.* **2002**, *12*, 81−85.
(64) Yu, J. C.; Yu, J.; Zhao, J. *Appl. Catal., B* **2002**, *36*, 31−43.
(65) Rengaraj, S.; Venkataraj, S.; Jee, S. H.; Kim, Y.; Tai, C.-w.; Repo, E.; Koistinen, A.; Ferancova, A.; Sillanpää, M. *Langmuir* **2010**, *27*, 352−358.
(66) Li, Q.; Guo, B.; Yu, J.; Ran, J.; Zhang, B.; Yan, H.; Gong, J. R. *J. Am. Chem. Soc.* **2011**, *133*, 10878−10884.
(67) Yu, J.; Yu, H.; Cheng, B.; Zhou, M.; Zhao, X. *J. Mol. Catal. A: Chem.* **2006**, *253*, 112−118.
(68) Chen, Z.; Zhang, N.; Xu, Y.-J. *CrystEngComm* **2013**, *15*, 3022−3030.
(69) He, B.-L.; Dong, B.; Li, H.-L. *Electrochem. Commun.* **2007**, *9*, 425−430.
(70) Zhang, Y.; Zhang, N.; Tang, Z.-R.; Xu, Y.-J. *ACS Nano* **2012**, *6*, 9777−9789.